Structural properties of liquid Ge_2Se_3: A first-principles study

Sébastien Le Roux,[1] Anita Zeidler,[2] Philip S. Salmon,[2] Mauro Boero,[1] Matthieu Micoulaut,[3] and Carlo Massobrio[1]
[1]*Institut de Physique et de Chimie des Matériaux de Strasbourg, 23 rue du Loess, BP43, F-67034 Strasbourg Cedex 2, France*
[2]*Department of Physics, University of Bath, Bath BA2 7AY, United Kingdom*
[3]*Laboratoire de Physique Théorique des Liquides, Université Pierre et Marie Curie, 4 Place Jussieu, F-75252 Paris Cedex 05, France*
(Received 25 March 2011; revised manuscript received 18 July 2011; published 13 October 2011)

The structural properties of liquid Ge_2Se_3were investigated by first-principles molecular dynamics using the Becke-Lee-Yang-Parr scheme for the treatment of the exchange-correlation functional in density functional theory. Our data for the total neutron structure factor and the total pair-distribution function are in excellent agreement with the experimental results. The structure is made predominantly (∼61%) from units comprising fourfold coordinated Ge atoms in the form of Ge-$GeSe_3$ or Ge-Se_4 motifs, but there is also a large variety of motifs in which Ge and Se are not fourfold and twofold coordinated, respectively. The miscoordinated atoms and homopolar bonds lead to a highly perturbed tetrahedral network, as reflected by diffusion coefficients that are larger than in the case of liquid $GeSe_2$. The network does, nevertheless, exhibit intermediate range order which is associated with the Ge-Ge correlations and which manifests itself by a first sharp diffraction peak in the total neutron structure factor. The evolution of the properties of Ge_xSe_{1-x} liquids ($0 \leqslant x \leqslant 1$) with composition is discussed.

DOI: 10.1103/PhysRevB.84.134203 PACS number(s): 61.25.Em, 61.20.Ja, 71.15.Pd

I. INTRODUCTION

There is widespread interest in the structure of disordered Ge_xSe_{1-x} ($0 \leqslant x \leqslant 1$) systems, partly because it is possible to control network properties such as the electrical conductivity, elastic constants, viscosity, and glass-forming ability by a continuous variation of the composition.[1–22] One important feature of these network structures is the establishment of intermediate range order (IRO) which is associated with the appearance of a first sharp diffraction peak (FSDP) located at a small scattering wave-vector $k \simeq 1$ Å^{-1} in the total structure factor measured in a diffraction experiment.[23] In the liquid state, the measured diffraction patterns show that IRO occurs in the range $0.15 \lesssim x \lesssim 0.40$ but is absent at $x = 0.5$.[3,4,15]

The changes in the network properties of liquid Ge_xSe_{1-x} or l-Ge_xSe_{1-x}, with increasing Ge content correspond to an evolution in character of the predominant structural motifs and their connectivity. For example, although the Ge-Se_4 tetrahedron is the main structural unit in both l-$GeSe_4$ and l-$GeSe_2$, the tetrahedra are mostly connected by shared Se atoms or Se chains in l-$GeSe_4$, whereas homopolar bonds and miscoordinations alter the regularity of the connections in l-$GeSe_2$.[7,19] By comparison, l-GeSe does not resemble a regular tetrahedral network and contains a wide variety of structural motifs where Ge-Se_3 and Se-Ge_3 units are the most frequently observed.[10] Thus it appears that there is a close relationship between the existence of a prevailing number of Ge-centered tetrahedral units and the appearance of intermediate range order.

A thorough understanding of the relationship between structure and composition can only be achieved by considering a representative set of systems on both the Se-rich ($x < 0.33$) and Ge-rich ($x > 0.33$) sides of the composition range. However, while much attention has been devoted to the Se-rich side, investigations of the Ge-rich side have focused only on l-GeSe.[10] This paucity of information for $x > 0.33$ prevents a complete atomic-scale picture of the structural trends to be attained. In particular, it would be beneficial to have detailed information on the expected transition between networks featuring intermediate range order (as in the case of l-$GeSe_4$ and l-$GeSe_2$) and networks in which this order is essentially absent (l-GeSe).

Given the above premises, the primary aim of the present work is to fill this gap by applying first-principles molecular dynamics (FPMD) to one representative case of l-Ge_xSe_{1-x} located within the composition range $0.33 < x < 0.50$. The computational approach follows the lines traced in an extensive body of research on the properties of disordered Ge_xSe_{1-x} networks.[6,7,10,11,17,19,20,24–30] We stress that a comparison of the network structures for different compositions has broad significance in the area of disordered systems. When the electronic structure is taken into explicit account, it is possible to understand the reasons why changes in the ratio of the two atomic species are responsible for modifications not only in the atomic but also in the chemical bonding properties.

Liquid Ge_2Se_3 is well suited to provide further insight into the microscopic origin of IRO since it is located at a composition, $x = 0.4$, that separates two systems having contrasting structures, namely, l-GeSe and l-$GeSe_2$. It also lies at the edge of the glass-forming region which extends over the range $0 \leqslant x \leqslant 0.43$ in the Ge_xSe_{1-x} system.[31] Neutron diffraction results for l-Ge_2Se_3 show that an FSDP is present in the total structure factor, its intensity being lower than in the case of l-$GeSe_2$.[3,15] The position of the first and second shells of nearest neighbors could also be extracted from the measured total pair-distribution function along with the mean coordination number. No information on the chemical identity of the nearest neighbors and corresponding coordination numbers could, however, be obtained because a full partial-structure-factor analysis was not made. We have therefore been motivated to apply first-principles molecular dynamics to investigate l-Ge_2Se_3 to gain a detailed description of both its structural and dynamical properties.

The paper is organized as follows. Our theoretical model is described in Sec. II and the results are compared to the

available neutron diffraction data in Sec. III. A detailed account of the structure of l-Ge_2Se_3 is then given, in both reciprocal space (Sec. IV) and real space (Sec. V), and a comparison is made with the structures of l-GeSe and l-$GeSe_2$. The interplay between the structural, dynamical, and electronic properties of l-Ge_2Se_3 is discussed in Sec. VI. Finally, the conclusions are summarized in Sec. VII.

II. THEORETICAL MODEL

Our simulations were performed at constant volume on a system containing $N = 120$ (48 Ge and 72 Se) atoms. We used a periodically repeated cubic cell of size 15.29 Å, corresponding to the experimental density of the liquid at a temperature $T = 1000$ K.[15] The system size is sufficiently large that the region of the observed FSDP is described by seven discrete wave-vectors, compatible with the periodicity of our supercell, where the minimum value $k_{\min} = 0.41$ Å^{-1} is significantly smaller than the position of the FSDP at $k_{\mathrm{FSDP}} \simeq 1$ Å^{-1}.[3]

The electronic structure was described within density functional theory (DFT) and evolved self-consistently during the motion.[32] We resort in this work to the generalized gradient approximation after Becke (B) for the exchange energy and Lee, Yang, and Parr (LYP) for the correlation energy.[33,34] A discussion on the reasons underpinning our choice of the BLYP exchange-correlation functional is given in recent papers where the Perdew and Wang (PW) and BLYP structures of liquid and glassy $GeSe_2$ are compared.[19,35,36] The BLYP approach gives a better description of the short-range properties due to a better account of valence electron localization effects. In our work, the valence electrons were treated explicitly, in conjunction with norm-conserving pseudopotentials of the Trouiller-Martins type to account for core-valence interactions.[37] The wave functions were expanded at the Γ point of the supercell on a plane-wave basis set with an energy cutoff $E_c = 20$ Ry.

The initial coordinates were provided by a configuration extracted from the fully equilibrated trajectories obtained for liquid $GeSe_2$ in Ref. 11 with an energy cutoff $E_c = 20$ Ry. To achieve the correct composition, the number of Ge atoms was changed to 48 by modifying the identity of eight randomly chosen Se atoms. To implement our first-principles molecular dynamics approach, we used a fictitious electron mass of 2000 a.u. (i.e., in units of $m_e a_0^2$, where m_e is the electron mass and a_0 is the Bohr radius) and a time step of $\Delta t = 0.24$ fs to integrate the equations of motion. Temperature control was implemented for both the ionic and electronic degrees of freedom by using Nosé-Hoover thermostats.[38–40] To lose memory of the initial configuration, we carried out simulations at $T = 2000$ K over a time period of 25 ps. During this time interval the Ge and Se atoms covered an average distance of 50 Å. After discarding this initial segment of the temporal trajectory, statistical averages were taken over an equilibrium trajectory covering a total time interval of 100 ps at $T = 1000$ K. The system was at thermal equilibrium for the entire length of this trajectory, as clearly demonstrated by the temporal behavior of the instantaneous value of the temperature shown in Fig. 1.

To appreciate the occurrence of an equilibrium region, it is useful to recall the expression for the standard deviation of the temperature $\sigma(T) = \sqrt{(2/3N)}\,T$.[38] In our case, $\sigma(T) \simeq 70$ K, which is consistent with the temperature fluctuations shown in Fig. 1. The error bar on the average quantities presented hereafter is smaller than 1%. Special attention has been given to the low wave-vector portion of the total and partial structure factors around $k \simeq 1$ Å^{-1}. As pointed out in Ref. 11, in the case of liquid $GeSe_2$ the height of the FSDP was affected by fluctuations as large as 20%. However, in the present case no substantial variation outside of the error bars was observed at any wave-vector value for any of the partial structure factors.

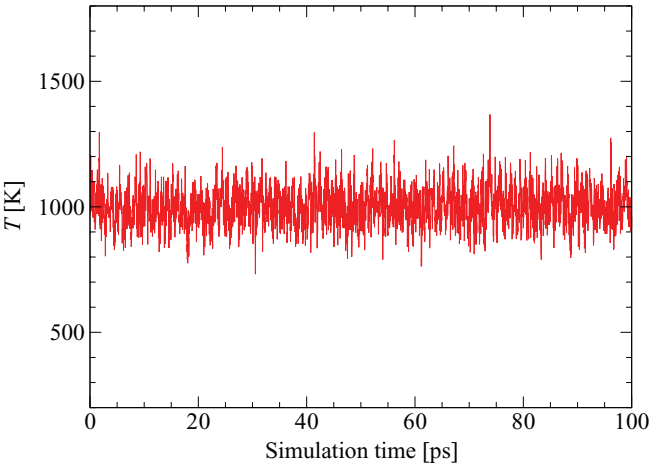

FIG. 1. (Color online) Dependence of the instantaneous value of the temperature on the simulation time for liquid Ge_2Se_3 at a mean temperature of 1000 K.

In the following, the results for liquid Ge_2Se_3 are compared in a systematic way with previous first-principles molecular dynamics data for the liquids $GeSe_4$, $GeSe_2$, and GeSe obtained within the same computational framework.[7,10,19] From the standpoint of the simulation methodology, the collection of equilibrium data for all of these systems has the following common points, i.e., (a) the choice of a plausible initial configuration, (b) the temporal evolution of the system over an extended time trajectory with the intent of losing memory of the initial configuration, (c) control of the average distance covered by the individual atoms during the temporal evolution sketched in (b) (typical distances range between 30 and 50 Å) and, finally, (d) the collection of equilibrium data at the temperature of interest. This step is substantiated by calculating the standard deviation of representative quantities (such as the temperature; see Fig. 1) to ensure that thermal equilibrium has been rigorously attained. For the specific details of each simulation, we refer to Ref. 7 for liquid $GeSe_4$, Ref. 19 for liquid $GeSe_2$, and Ref. 10 for liquid GeSe.

The results obtained from the present work are most readily compared with those obtained for the liquids $GeSe_2$ and GeSe since they correspond to compositions that lie on the Se- and Ge-rich sides of Ge_2Se_3, respectively. However, while the results for the first two systems were obtained within the BLYP framework, the results for liquid GeSe were obtained by using the PW approach.[10] For this reason, an additional simulation run (lasting 10 ps) was produced for liquid GeSe at $T = 1000$ K by using the BLYP functional. While a complete assessment of the effect of this functional on the properties of liquid GeSe is not within the scope of the present study,

some preliminary results on the coordination numbers will be presented in Sec. V B.

III. NEUTRON TOTAL STRUCTURE FACTOR AND TOTAL PAIR-CORRELATION FUNCTION

The total neutron structure factor $S_T(k)$ is defined by

$$S_T(k) - 1 \equiv \sum_{\alpha=1}^{n}\sum_{\beta=1}^{n} \frac{c_\alpha c_\beta b_\alpha b_\beta}{\langle b\rangle^2}\left[S^{FZ}_{\alpha\beta}(k) - 1\right], \qquad (1)$$

where α and β denote the chemical species, $n = 2$ is the number of different chemical species, c_α and b_α are the atomic fraction and coherent neutron-scattering length of chemical species α, $\langle b\rangle = c_{Ge}b_{Ge} + c_{Se}b_{Se}$ is the mean coherent neutron-scattering length, and $S^{FZ}_{\alpha\beta}(k)$ is a Faber-Ziman (FZ) partial structure factor. The coherent neutron-scattering lengths for Ge and Se of natural isotopic abundance are $b_{Ge} = 8.185$ fm and $b_{Se} = 7.970$ fm.[15] The corresponding real-space information is given by the total pair-distribution function

$$g_T(r) - 1 = \frac{1}{2\pi^2 n_0 r}\int_0^\infty dk\, k\,[S_T(k) - 1]\sin(kr)$$
$$= \sum_{\alpha=1}^{n}\sum_{\beta=1}^{n} \frac{c_\alpha c_\beta b_\alpha b_\beta}{\langle b\rangle^2}[g_{\alpha\beta}(r) - 1], \qquad (2)$$

where n_0 is the atomic number density and $g_{\alpha\beta}(r)$ is a partial pair-distribution function.

In Fig. 2 we compare the calculated total neutron structure factor $S^{th}_T(k)$ for l-Ge_2Se_3 with its experimental counterpart $S^{exp}_T(k)$.[3] The agreement is very good over the entire range of wave-vectors, both curves being essentially superposed for $k \geqslant 3$ Å^{-1}. There is, however, a small shift of the FSDP in $S^{th}_T(k)$ toward higher k values and a small shift in the peak at $k \simeq 2$ Å^{-1} toward lower k values. The FSDP of $S^{th}_T(k)$ is broader by comparison with experiment.

The measured and calculated total pair-distribution functions for l-Ge_2Se_3 are compared in Fig. 3. The experimental result, $g^{exp}_T(r)$, was obtained by Fourier transforming the

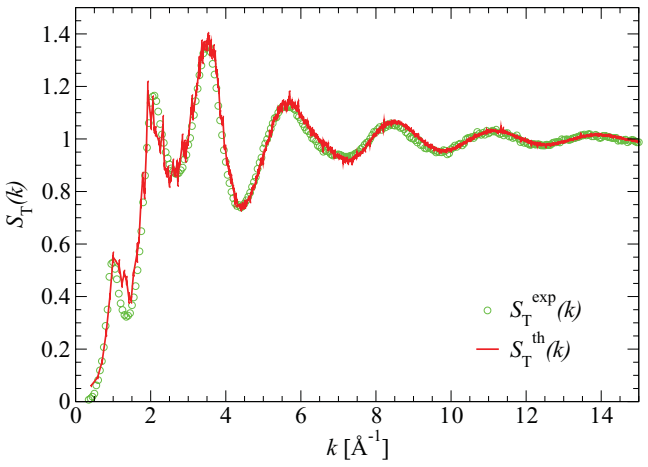

FIG. 2. (Color online) Total neutron structure factor for liquid Ge_2Se_3 at $T = 1000$ K. The experimental result $S^{exp}_T(k)$ given in Ref. 3 (green circles) is compared to the calculated function $S^{th}_T(k)$ (solid red curve).

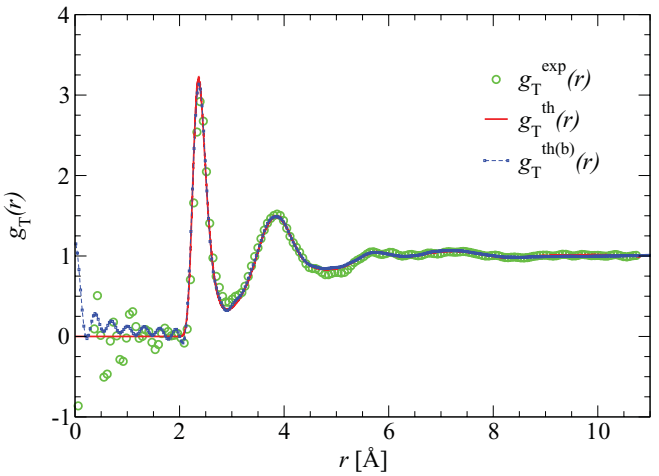

FIG. 3. (Color online) Total pair-distribution function for liquid Ge_2Se_3 at $T = 1000$ K. The experimental function $g^{exp}_T(r)$ of Ref. 3 (green circles) was obtained by Fourier transforming the measured total structure factor $S^{exp}_T(k)$ (see Fig. 2) with a cutoff value $k_{max} = 19.95$ Å^{-1}. The same procedure was applied to the computed function $S^{th}_T(k)$ (see Fig. 2) to obtain $g^{th(b)}_T(r)$ (broken blue curve with square symbols). The total pair-distribution function $g^{th}_T(r)$ (solid red curve) is the result of a direct calculation from the real-space coordinates.

reciprocal space data set with an upper limit of integration set to $k_{max} = 19.95$ Å^{-1} in Eq. (2). This upper limit results from the finite measurement window function of the diffractometer and leads to spurious oscillations at $r < 2$ Å. Two approaches were used to obtain the total pair-distribution function from the FPMD results. In the first, the function $g^{th}_T(r)$ was calculated directly from the atomic coordinates of the simulation. In the second, the experimental procedure was followed such that the calculated total structure factor $S^{th}_T(k)$ was Fourier transformed with k_{max}=19.95 Å^{-1} to give the function $g^{th(b)}_T(r)$. For $r > 2$Å, the only notable difference between $g^{exp}_T(r)$ and either $g^{th}_T(r)$ or $g^{th(b)}_T(r)$ is the larger intensity of the main peak in $g^{th}_T(r)$.

IV. RECIPROCAL SPACE PROPERTIES

A. Faber-Ziman partial structure factors

The calculated FZ partial structure factors for liquid Ge_2Se_3 are shown in Fig. 4 where a comparison is made with the functions calculated for liquid GeSe at $T = 1000$ K and for liquid $GeSe_2$ at $T = 1050$ K. In Fig. 4, a comparison is also made with the experimental data sets for l-GeSe and l-$GeSe_2$, which were measured by using the method of isotope substitution in neutron diffraction, since these are available in the literature.[2,9] A detailed discussion of the theoretical and experimental results for l-GeSe and l-$GeSe_2$ is given in Refs. 10 and 19, respectively.

In moving from l-GeSe to l-Ge_2Se_3, the most striking feature in Fig. 4 is the appearance of an FSDP in the $S^{FZ}_{GeGe}(k)$ partial structure factor. Hence, Ge-Ge correlations extending well beyond the nearest-neighbor distances are responsible for the onset of intermediate range ordering in l-Ge_2Se_3. The relative heights of the FSDP in $S^{FZ}_{GeGe}(k)$ for l-Ge_2Se_3 and l-$GeSe_2$, and the absence of this feature for l-GeSe, suggests the development of a predominant Ge-centered tetrahedral

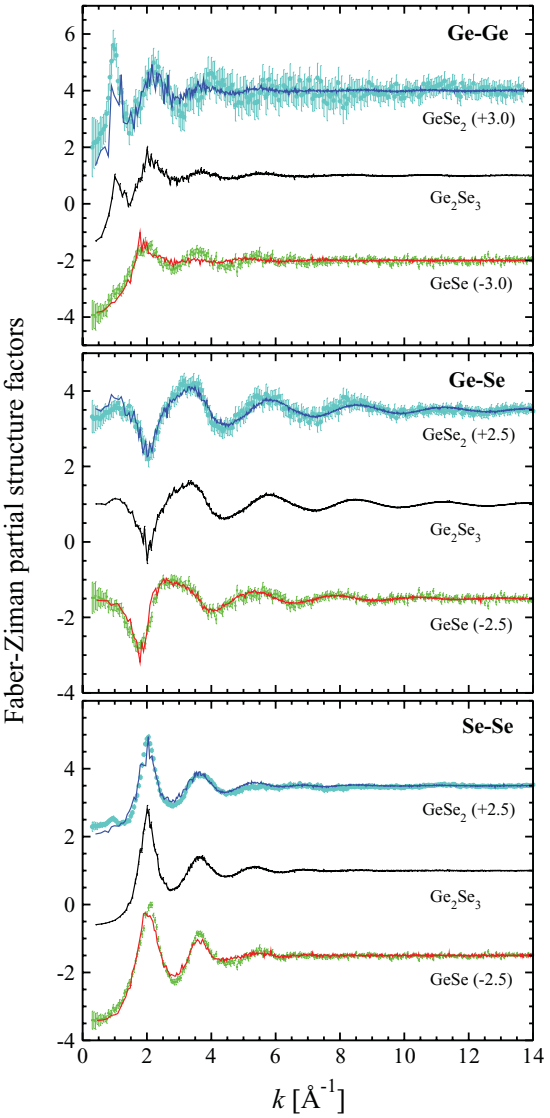

FIG. 4. (Color online) The Faber-Ziman partial structure factors $S^{\mathrm{FZ}}_{\mathrm{GeGe}}(k)$ (top panel), $S^{\mathrm{FZ}}_{\mathrm{GeSe}}(k)$ (middle panel), and $S^{\mathrm{FZ}}_{\mathrm{SeSe}}(k)$ (bottom panel) for the liquids $GeSe_2$, Ge_2Se_3, and GeSe. For l-$GeSe_2$, the FPMD results (Ref. 19) (solid blue curves) are compared with the experimental results (Ref. 2) (light blue symbols) where both sets of data are shifted upward by the indicated values. For l-Ge_2Se_3, in the absence of experimental results, only the FPMD results of the present work are shown (solid black curves). For l-GeSe, the FPMD results (Ref. 10) (solid red curves) are compared with the experimental results (Ref. 9) (green symbols) where both sets of data are shifted downward by the indicated values.

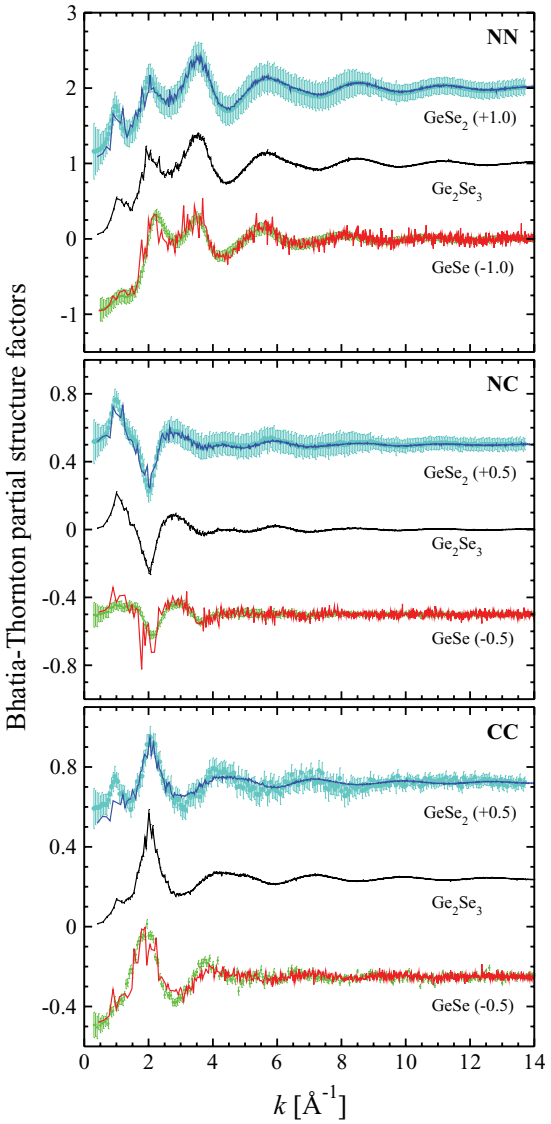

FIG. 5. (Color online) The Bhatia-Thornton partial structure factors $S_{\mathrm{NN}}(k)$ (top panel), $S_{\mathrm{NC}}(k)$ (middle panel), and $S_{\mathrm{CC}}(k)$ (bottom panel) for the liquids $GeSe_2$, Ge_2Se_3, and GeSe. For l-$GeSe_2$, the FPMD results (Ref. 19) (solid blue curves) are compared with the experimental results (Ref. 2) (light blue symbols) where both sets of data are shifted upward by the indicated values. For l-Ge_2Se_3, in the absence of experimental results, only the FPMD results of the present work are shown (solid black curves). For l-GeSe, the FPMD results (Ref. 10) (solid red curves) are compared with the experimental results (Ref. 9) (green symbols) where both sets of data are shifted downward by the indicated values.

motif with increasing Se content. This is supported by an analysis of the structures of l-$GeSe_2$ and l-GeSe (Refs. 10 and 19) where it is found that l-GeSe has little in common with the tetrahedral network of l-$GeSe_2$ but comprises, instead, a substantial proportion of highly distorted Ge-Se_3, Se-Ge_3, and far from tetrahedral-like Ge-$GeSe_3$ units.

B. Bhatia-Thornton partial structure factors

In Fig. 5 we compare the Bhatia-Thornton (BT) number-number, $S_{\mathrm{NN}}(k)$, number-concentration, $S_{\mathrm{NC}}(k)$, and concentration-concentration, $S_{\mathrm{CC}}(k)$, partial structure factors[41,42] for l-Ge_2Se_3, l-$GeSe_2$, and l-GeSe. In terms of the Bhatia-Thornton structure factors, the total neutron structure factor reads

$$S_{\mathrm{T}}(k) = S_{\mathrm{NN}}(k) + A\,[S_{\mathrm{CC}}(k)/c_{\mathrm{Ge}}\,c_{\mathrm{Se}} - 1] + B\,S_{\mathrm{NC}}(k), \quad (3)$$

where $A = c_{\mathrm{Ge}}c_{\mathrm{Se}}\Delta b^2/\langle b\rangle^2$, $B = 2\Delta b/\langle b\rangle$, and $\Delta b = b_{\mathrm{Ge}} - b_{\mathrm{Se}}$.[12] For the compositions $c_{\mathrm{Ge}} = 0.33$, 0.4, and 0.5, the coefficient $A \lesssim 1.8\times10^{-4}$ and the coefficient $B \lesssim 0.054$ due to the similarity between the scattering lengths of Ge and Se. Also, as shown in Fig. 5, $S_{\mathrm{NC}}(k)$ and $S_{\mathrm{CC}}(k)$ show a limited

range of variation with composition with $|S_{NC}(k)| < 0.6$ and $S_{CC}(k) < 0.6$. $S_T(k)$ is, therefore, a very good approximation for $S_{NN}(k)$, i.e., $|S_T(k) - S_{NN}(k)| < 0.025$. In consequence, the results for $S_T(k)$ shown in Fig. 2 hold equally well for $S_{NN}(k)$ shown in Fig. 5, a conclusion that is supported by experiments on l-GeSe and l-$GeSe_2$.[15]

The $S_{NC}(k)$ and FZ partial structure factors are related by the expression

$$S_{NC}(k) = c_{Ge}c_{Se}\{c_{Ge}[S^{FZ}_{GeGe}(k) - S^{FZ}_{GeSe}(k)] - c_{Se}[S^{FZ}_{SeSe}(k) - S^{FZ}_{GeSe}(k)]\}. \quad (4)$$

In the region of the FSDP, the $c_{Ge}S^{FZ}_{GeGe}(k)$ term leads to an intense positive contribution to $S_{NC}(k)$ in the cases of l-Ge_2Se_3 and l-$GeSe_2$ but not in the case of l-GeSe for which an FSDP is absent in all of the FZ partial structure factors. The contributions to $S_{NC}(k)$ arising from both of the $S^{FZ}_{GeSe}(k)$ terms largely offset one another since they have opposite signs. The trough in $S_{NC}(k)$ at $k \sim 2$ Å^{-1}, which is common to l-Ge_2Se_3, l-$GeSe_2$, and l-GeSe, is mostly due to the main peak in $S_{SeSe}(k)$.

The $S_{CC}(k)$ and FZ partial structure factors are related by the expression

$$S_{CC}(k) = c_{Ge}c_{Se}(1 + c_{Ge}c_{Se}\{[S^{FZ}_{GeGe}(k) - S^{FZ}_{GeSe}(k)] + [S^{FZ}_{SeSe}(k) - S^{FZ}_{GeSe}(k)]\}). \quad (5)$$

Our calculated $S_{CC}(k)$ for l-Ge_2Se_3 features a small peak in the FSDP region which points to concentration fluctuations on the scale of the IRO (Ref. 43) which, in systems like l-$GeSe_2$, is indicative of a small departure from chemical order.[28]

When taken together, the reciprocal space data sets for l-Ge_2Se_3 suggest a network structure made from Ge-centered tetrahedral units with a moderate number of miscoordinated atoms. More information on this structure, including the role played by Ge-Ge homopolar bonds, is provided by an analysis of the real-space data sets.

V. REAL-SPACE PROPERTIES

A. Pair distribution functions

In Fig. 6 we display the calculated partial pair-distribution functions $g_{\alpha\beta}(r)$ for l-Ge_2Se_3 together with the calculated functions for l-GeSe and l-$GeSe_2$.[10,19] The experimental data sets for l-GeSe and l-$GeSe_2$ are also shown.[2,9]

For l-Ge_2Se_3 and l-$GeSe_2$ the main peak in $g_{GeSe}(r)$ occurs at 2.36 Å and is of comparable intensity for both of these materials, consistent with the appearance of a predominant Ge-centered tetrahedral motif. For l-GeSe the intensity of the main peak is much smaller, its position is shifted to a higher value of 2.57 Å, and the peak does not approach the $g_{GeSe}(r = 0) = 0$ limit on its high r side. This is consistent with the variety of Ge and Se coordination environments that characterize the short-range order in this system.[9,10]

In the case of l-Ge_2Se_3, the small peak at $\simeq 2.4$ Å in $g_{SeSe}(r)$ results from the occurrence of Se-Se homopolar bonds. These Se-Se contacts are not expected on the basis of a chemically ordered network (CON) model for l-Ge_xSe_{1-x} with $x > 0.33$.[15] The shapes and intensities of the $g_{SeSe}(r)$ functions for each liquid are quite similar in the interval $3 < r$ (Å) < 5. i.e., there is little sensitivity of the Se-Se distances within

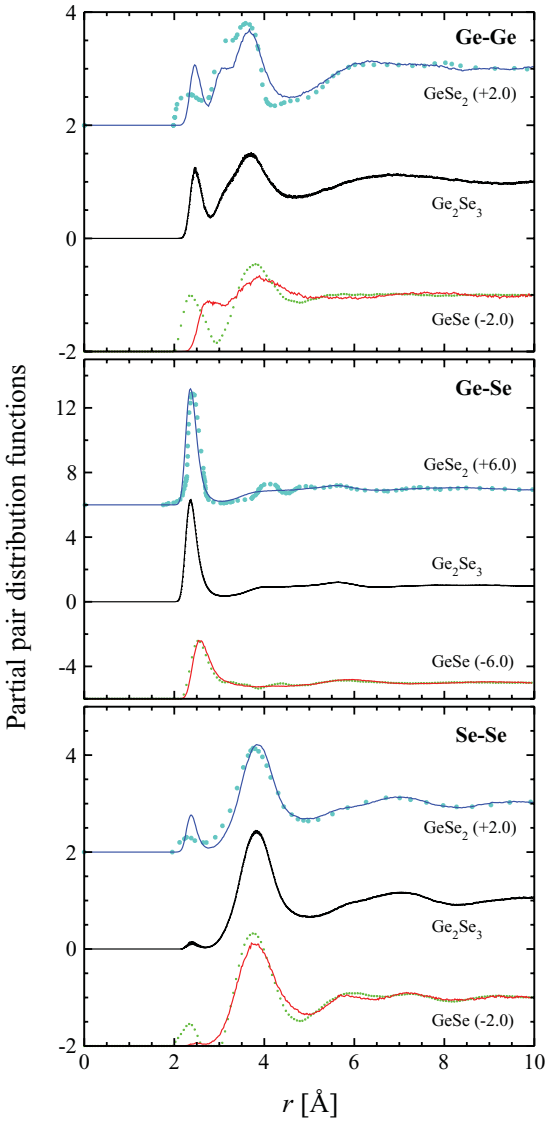

FIG. 6. (Color online) The partial pair-distribution functions $g_{GeGe}(r)$ (top panel), $g_{GeSe}(r)$ (middle panel) and $g_{SeSe}(r)$ (bottom panel) for the liquids $GeSe_2$, Ge_2Se_3 and GeSe. For l-$GeSe_2$, the FPMD results[19] (solid blue curves) are compared with the experimental results[2] (light blue symbols) where both sets of data are shifted upward by the indicated values. For l-Ge_2Se_3, in the absence of experimental results, only the FPMD results of the present work are shown (solid black curves). For l-GeSe, the FPMD results[10] (solid red curves) are compared with the experimental results[9] (green symbols) where both sets of data are shifted downward by the indicated values.

structural motifs to changes in the liquid composition or to the presence (or absence) of IRO.

For l-Ge_2Se_3, $g_{GeGe}(r)$ features a well-defined first peak at $r = 2.47$ Å which arises from Ge-Ge homopolar bonds. The second peak has contributions from edge-sharing motifs at a distance $r \simeq 3$ Å and corner-sharing motifs at larger distances. A quench of the liquid to the glass would lead to a clearer resolution of the edge-sharing and corner-sharing contributions as shown by studies of other Ge_xSe_{1-x} systems.[17,30]

It is worthwhile pointing out that the differences between theory and experiment for l-GeSe and l-$GeSe_2$ arise from an

overestimate of the metallic character of the bonding.[10,19] In the case of l-$GeSe_2$ a partial correction for this deficiency was made by using the BLYP exchange-correlation functional and it is the FPMD results obtained by using this scheme[19] that are presented herein. In the case of l-GeSe, the available FPMD results were obtained by using the PW exchange-correlation functional.[10] For this system, it is not so obvious that use of the BLYP scheme will lead to better agreement between theory and experiment since it is a more metallic material as indicated by an increased electrical conductivity.[44,45] Indeed, preliminary results for the coordination numbers of l-GeSe, obtained by using the BLYP scheme (see Sec. V B), indicate that the essence of the atomic-scale description of this liquid is not changed when switching from the PW to the BLYP exchange-correlation functional.[46]

B. Coordination numbers

The coordination numbers $\bar{n}_{\alpha\beta}$ for the liquids $GeSe_4$, $GeSe_2$, Ge_2Se_3, and GeSe are listed in Table I. They are defined as the mean number of nearest neighbors of type β around an atom of type α within an integration range that includes distances up to the first minimum of the total pair-distribution function. The values of $\bar{n}_{GeGe}$ and $\bar{n}_{GeSe}$ for l-Ge_2Se_3 are higher and lower than in the case of l-$GeSe_2$, respectively, due to a larger number of Ge-Ge homopolar bonds and the inability of Ge atoms to form a predominant Ge-Se_4 motif owing to a lack of Se atoms. The non-negligible value of $\bar{n}_{SeSe}$ suggests that Se n-mers can form even in Ge-rich compositions of l-Ge_xSe_{1-x} (i.e., $x > 0.33$), the formation of chains of Se atoms being well established in systems like liquid and glassy $GeSe_4$.[7,20] As an illustration of the network topology in l-Ge_2Se_3 we provide in Fig. 7 a snapshot of the structure at a given instant of time along the equilibrium trajectory.

TABLE I. The first peak position (FPP) and second peak position (SPP) in $g_{\alpha\beta}(r)$ and the nearest-neighbor coordination numbers $\bar{n}_{\alpha\beta}$ obtained from FPMD models of the liquids $GeSe_4$ (Ref. 7), $GeSe_2$ (Ref. 19), Ge_2Se_3 (present work), and GeSe (Ref. 10). The coordination numbers $\bar{n}_{\alpha\beta}$ for l-Ge_2Se_3 were obtained by using an integration range of 0–2.9 Å where the upper limit corresponds to the first minimum in the total pair-distribution function. The predictions of the CON and RCN models are also listed (Ref. 15).

$g_{\alpha\beta}(r)$	Liquid	FPP (Å)	SPP (Å)	$\bar{n}_{\alpha\beta}$	$\bar{n}_{\alpha\beta}$ (CON)	$\bar{n}_{\alpha\beta}$ (RCN)
$g_{GeGe}(r)$	$GeSe_4$	2.54	3.73	0.06	0	1.3333
	$GeSe_2$	2.45	3.67	0.22	0	2
	Ge_2Se_3	2.47	3.70	0.48	1	2.2857
	GeSe	2.77	3.87	0.8	2	2.6667
$g_{GeSe}(r)$	$GeSe_4$	2.38	3.77	3.87	4	2.6667
	$GeSe_2$	2.36	5.67	3.55	4	2
	Ge_2Se_3	2.36	5.65	3.15	3	1.7143
	GeSe	2.57		2.94	2	1.3333
$g_{SeGe}(r)$	$GeSe_4$	2.38	3.77	0.97	1	0.6666
	$GeSe_2$	2.36	5.67	1.78	2	1
	Ge_2Se_3	2.36	5.65	2.10	2	1.1429
	GeSe	2.57		2.94	2	1.3333
$g_{SeSe}(r)$	$GeSe_4$	2.30	3.85	1.04	1	1.3333
	$GeSe_2$	2.38	3.83	0.33	0	1
	Ge_2Se_3	2.39	3.81	0.08	0	0.8571
	GeSe	2.50	3.80	0.1	0	0.6667

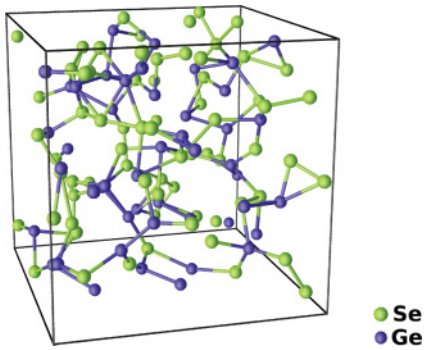

FIG. 7. (Color online) Snapshot of the structure of the FPMD model for liquid Ge_2Se_3 where the Ge atoms are (dark) blue and the Se atoms are (light) green.

The total coordination numbers for Ge and Se are given by $\bar{n}_{Ge} = \bar{n}_{GeGe} + \bar{n}_{GeSe}$ and $\bar{n}_{Se} = \bar{n}_{SeSe} + \bar{n}_{SeGe}$, respectively, where $\bar{n}_{SeGe}/c_{Ge} = \bar{n}_{GeSe}/c_{Se}$. The average coordination number irrespective of chemical species type is given by the expression $\bar{n} = c_{Ge}(\bar{n}_{GeGe} + \bar{n}_{GeSe}) + c_{Se}(\bar{n}_{SeSe} + \bar{n}_{SeGe})$. The upper value of the integration range (2.9 Å) used to obtain $\bar{n}$ corresponds to the first minimum of the total pair-distribution function as employed in Ref. 15. The FPMD values of these parameters are shown in Table II together with the results obtained for the liquids $GeSe_4$, $GeSe_2$, Ge_2Se_3, and GeSe. A comparison is also made with the measured $\bar{n}$ values and with the $\bar{n}$ values expected from the "8-N" rule where Ge atoms are fourfold coordinated and Se atoms are twofold coordinated. Within the framework of this rule, there are two simple models for the network structure of l-Ge_xSe_{1-x}.[15] In the chemically ordered network (CON) model, Ge-Se bonds are favored such that only Ge-Se and Ge-Ge bonds are allowed for compositions with $x > 0.33$, while only Ge-Se and Se-Se bonds are allowed for compositions with $x < 0.33$. In the random covalent network (RCN) model there is a purely statistical distribution of bond types such that Se-Se bonds are allowed for $x > 0.33$ and Ge-Ge bonds are allowed for $x < 0.33$.

The FPMD and measured values for $\bar{n}$ are in accord with the 8-N rule in the case of l-$GeSe_4$, l-$GeSe_2$, and l-Ge_2Se_3 but not in the case of l-GeSe. The calculated values of $\bar{n}_{Ge}$ and $\bar{n}_{Se}$ show that, while in l-$GeSe_4$ and l-$GeSe_2$ the Ge and Se atoms are essentially fourfold and twofold coordinated, respectively, there is an increasing departure from the 8-N rule with increasing Ge content. The $\bar{n}_{\alpha\beta}$ values given in Table I point to a structure for l-$GeSe_4$ in which Ge-Se_4 tetrahedra are embedded in a chemically ordered network. Although Ge-Se_4 tetrahedra are also the predominant structural motifs in l-$GeSe_2$, there is partial chemical disorder as indicated by the appearance of Ge-Ge homopolar bonds. In the case of l-Ge_2Se_3, the appearance of Ge-Ge homopolar bonds is consistent with the notion of chemical order within the framework of the 8-N rule but the calculated $\bar{n}_{GeGe}$ value is less than expected on the assumption of a CON. The 8-N rule does not act as an accurate guide to the structure of l-GeSe and, for this system, the CON and RCN models do not give a good account of the FPMD results. We draw attention to the fact that the latter holds for both of the exchange-correlation schemes employed to study

TABLE II. The total coordination numbers for Ge, $\bar{n}_{Ge}$, and Se, $\bar{n}_{Se}$, in l-Ge_2Se_3 as calculated by using a cut-off distance of 2.9 Å. The results are compared with those obtained from FPMD models of the liquids $GeSe_4$ (Ref. 7), $GeSe_2$ (Ref. 19), and GeSe (Ref. 10). The calculated average coordination number, $\bar{n}$, for each system is also listed and the values are compared with the experimental results of Ref. 15 and with the expectations of the 8-N rule. For liquid GeSe, two sets of values are given, differing by the expression used for the exchange-correlation functional (PW or BLYP; see the text) within DFT.

Liquid	$\bar{n}_{Ge}$	$\bar{n}_{Se}$	$\bar{n}$	$\bar{n}$(exp)	$\bar{n}$ (8-N)
$GeSe_4$	3.93	2.01	2.39	2.44(6)[a]	2.4
$GeSe_2$	3.77	2.11	2.66	2.6(1)	2.67
Ge_2Se_3	3.63	2.18	2.76	2.8(2)	2.8
GeSe (PW)	3.74	3.04	3.39	3.5(3)	3
GeSe (BLYP)	3.87	2.74	3.30	3.5(3)	3

[a]Value obtained for the glass.

l-GeSe. The calculated values of $\bar{n}_{Ge}$ and $\bar{n}_{Se}$ for l-GeSe are only moderately affected by the enhanced valence electron localization properties of the BLYP functional, resulting in an average coordination number of $\bar{n} = 3.30$, which is only 3% lower than the corresponding PW value of $\bar{n} = 3.39$ (see Table II).

To explore the ordering in more detail, it is instructive to consider the generalized Warren-Cowley[47,48] and the Cargill-Spaepen[49] short-range chemical order parameters defined by $\alpha_w \equiv 1 - \bar{n}_{GeSe}/c_{Se}\bar{n}_w$ and $\eta \equiv \bar{n}_{GeSe}\bar{n}/c_{Se}\bar{n}_{Ge}\bar{n}_{Se} - 1$, respectively, where $\bar{n}_{GeSe}/c_{Se} = \bar{n}_{SeGe}/c_{Ge}$ and $\bar{n}_w = c_{Se}\bar{n}_{Ge} + c_{Ge}\bar{n}_{Se}$. To compare the degree of chemical ordering in systems with different compositions and coordination numbers, it is convenient to define the normalized order parameters $\alpha_w^0 = \alpha_w/\alpha_w^{max}$ and $\eta^0 = \eta/\eta^{max}$, where the superscript max corresponds to the case when, for fixed composition and coordination numbers $\bar{n}_{Ge}$ and $\bar{n}_{Se}$, the heteropolar coordination number is a maximum such that either $\bar{n}_{Ge} = \bar{n}_{GeSe}$ with $\bar{n}_{GeGe} = 0$ or $\bar{n}_{Se} = \bar{n}_{SeGe}$ with $\bar{n}_{SeSe} = 0$. The normalization parameters are given by $\eta^{max} = c_{Se}\bar{n}_{Se}/c_{Ge}\bar{n}_{Ge}$ if $c_{Ge}\bar{n}_{Ge} > c_{Se}\bar{n}_{Se}$ or $\eta^{max} = c_{Ge}\bar{n}_{Ge}/c_{Se}\bar{n}_{Se}$ if $c_{Ge}\bar{n}_{Ge} < c_{Se}\bar{n}_{Se}$ (Ref. 49), while $\alpha_w^{max} = 1 - \bar{n}_{Ge}/c_{Se}\bar{n}_w$ if $c_{Ge}\bar{n}_{Ge} > c_{Se}\bar{n}_{Se}$ or $\alpha_w^{max} = 1 - \bar{n}_{Se}/c_{Ge}\bar{n}_w$ if $c_{Ge}\bar{n}_{Ge} < c_{Se}\bar{n}_{Se}$.[50] The chemical order parameters for FPMD models of the liquids $GeSe_4$, $GeSe_2$, Ge_2Se_3, and GeSe are given in Table III where a comparison is also made with the values expected from the 8-N rule. On the basis of these parameters, l-$GeSe_4$ forms the most chemically ordered network and the model for l-Ge_2Se_3 appears to be more chemically ordered than the model for l-$GeSe_2$.

C. Structural units

To provide a more complete description of the network we identify the individual α-l structural units where an atom of species α (Ge or Se) is l-fold coordinated to other atoms. To clarify this notation, Ge-$GeSe_3$ represents a Ge atom that is connected to one other Ge atom and three Se atoms, while Ge-Se_4 represents a Ge atom that is connected to four Se atoms. The proportion of a specific unit, $\bar{n}_\alpha(l)$, is found by taking the ratio of the mean number of its occurrences in the different simulation configurations to the total number of atoms of type α within the model. Each type of unit will have an average lifetime, τ, as determined from the average number of consecutive configurations for which this type of unit is found. The identity of a unit can therefore fluctuate and we define the total time of existence, δ, of a given type of unit by counting the number of its occurrences, irrespective of the time separating different configurations. Very high values of δ (close to 100% of the total time of the equilibrium trajectory) are perfectly consistent with small values of τ, since bond breaking and reforming can be extremely rapid, thus affecting the temporal stability of a given unit. Bonds are deemed to be formed when the interatomic distance for a given pair of atoms is smaller than 2.9 Å, corresponding to the first minimum in the total pair-distribution function, a choice that is consistent with similar analyses carried out for l-$GeSe_4$, l-$GeSe_2$, and l-GeSe.[7,10,11] The proportion of units $\bar{n}_\alpha(l)$ and the associated times δ and τ are summarized in Table IV.

TABLE III. The generalized Warren-Cowley and the Cargill-Spaepen short-range chemical order parameters for FPMD models of the liquids $GeSe_4$ (Ref. 7), $GeSe_2$ (Ref. 19), Ge_2Se_3 (present work), and GeSe (Ref. 10). The parameters are normalized (see the text) and are compared to the values expected from the 8-N rule. For liquid GeSe, two sets of values are given, differing by the expression used for the exchange-correlation functional (PW or BLYP; see the text) within DFT.

Liquid	α_w^0	η^0	α_w^0 (CON)	α_w^0 (RCN)	η^0 (CON)	η^0 (RCN)
$GeSe_4$	0.20	0.95	0.219	−0.042	1	0
$GeSe_2$	0.68	0.88	1.000	−0.125	1	0
Ge_2Se_3	0.73	0.92	0.519	−0.099	1	0
GeSe (PW)	0.61	0.93	0.200	−0.067	1	0
GeSe (BLYP)	0.47	0.95	0.200	−0.067	1	0

Our model is characterized by high proportions of Ge-$GeSe_3$ units containing Ge-Ge homopolar bonds (30.8%), Ge-Se_4 units (30.2%), and Se-Ge_2 units (75.6%). The majority of Ge atoms (64%) have four nearest neighbors, while the majority of Se atoms (79.4%) have two nearest neighbors. The presence of a large number of fourfold coordinated Ge atoms supports the notion that the FSDP in $S_{GeGe}(k)$ is linked to the formation of a predominant tetrahedral unit. By contrast, in liquid GeSe only $\simeq$43% of the Ge atoms have four nearest neighbors (see Table IV), i.e., within the family of Ge_xSe_{1-x} liquids there is a transition between two substantially different kinds of network when x is larger than 0.4.

The question arises as to the impact that the different coordination units have on the properties of the liquid, especially in the case of under- and overcoordinated Ge and Se atoms. In this respect, small δ values indicate highly transient motifs, such as Ge-GeSe and Ge-Se_5 in the case of the Ge-centered units and Se-Se, Se-Se_2, and Se-Ge_2Se_2 in the case of the Se-centered units. Motifs with significantly high δ values ($\geqslant$70% of the total time of the equilibrium trajectory) can be identified as dynamically stable or unstable according to their lifetime τ. Very short lifetimes ($\tau < 1.0$% of the total time of the equilibrium trajectory) can be understood in terms of very fast processes involving the creation and destruction of chemical bonds at a high rate.

TABLE IV. The proportion $\bar{n}_\alpha(l)$, overall presence time δ, and average lifetime τ, of the different coordination units in liquid Ge_2Se_3. The identity of the α atom (Ge or Se) at the center of a unit is given in bold font and the identity of the l nearest neighbors is given in the second column. The lifetimes are expressed as a fraction of the total time of the equilibrium trajectory over which statistical averages were taken (100 ps). The proportion $\bar{n}_\alpha(l)$ of the different coordination units for the case of liquid GeSe (obtained by using the BLYP approach) is given in parentheses next to the values for liquid Ge_2Se_3.

		Proportion $\bar{n}_\alpha(l)$(%)	Overall presence time δ (%)	Lifetime τ (%)
Ge atom				
$l=2$	Se_2	9.0(5.4)	98.7	1.4
	GeSe	0.6(0.8)	19.2	0.1
$l=3$	$GeSe_2$	5.2(10.12)	89.9	0.4
	Se_3	16.5(21.4)	99.9	10.0
$l=4$	$GeSe_3$	30.8(23.2)	99.8	6.2
	Ge_2Se_2	3.0(7.3)	92.3	0.9
	Se_4	30.2(12.2)	99.3	4.5
$l=5$	Ge_2Se_3	1.4(5.3)	40.1	0.1
	$GeSe_4$	2.9(6.9)	64.7	0.1
	Se_5	0.2(1.7)	9.1	0.1
Se atom				
$l=1$	Ge	2.0(0.7)	17.3	0.1
	Se	<0.1(<0.1)	1.8	<0.1
$l=2$	Se_2	0.2(0.1)	3.1	0.1
	SeGe	3.6(0.9)	33.5	0.1
	Ge_2	75.6(21.2)	62.2	0.1
$l=3$	Se_2Ge	0.3(0.2)	5.13	0.1
	$SeGe_2$	2.8(3.0)	17.7	0.1
	Ge_3	14.9(48.7)	36.7	0.1
$l=4$	$SeGe_3$	0.2(3.3)	3.9	<0.1
	Ge_4	0.3(18.6)	18.6	0.1
	Ge_2Se_2	0.1(0.4)	1.6	<0.1

D. Bond-angle distributions

The bond-angle distributions θ_{GeSeGe} and θ_{SeGeSe} for l-$GeSe_2$, l-Ge_2Se_3, and l-GeSe are shown in Fig. 8. The similarity between the distributions for l-$GeSe_2$ and l-Ge_2Se_3 arises from the formation of a predominantly tetrahedral network and there is a striking difference with the distributions for l-GeSe which can be accounted for by the disappearance of tetrahedral ordering. In the case of l-$GeSe_2$ and l-Ge_2Se_3, the peaks in θ_{GeSeGe} at about 80° and 100° [see Fig. 8(a)] can be attributed to the formation of edge-sharing and corner-sharing tetrahedra, respectively.[11] The θ_{SeGeSe} bond-angle distribution for l-Ge_2Se_3 is symmetrical around a peak position at 105° [Fig. 8(b)] and follows very closely the shape of the θ_{SeGeSe} curve for l-$GeSe_2$. In both cases, the coexistence of tetrahedral motifs with a variety of miscoordinated units results in a small shift of the maximum when compared to perfect tetrahedral geometry. In the case of l-GeSe, the simultaneous occurrence of a maximum at ∼90° in both the θ_{GeSeGe} and θ_{SeGeSe} bond-angle distributions was interpreted in terms of the existence of chemically ordered fourfold rings but in the absence of tetrahedral order.[10] Indeed, the PW results for l-GeSe show that only 43.2% of the Ge atoms are fourfold coordinated and that there are sizable percentages of twofold

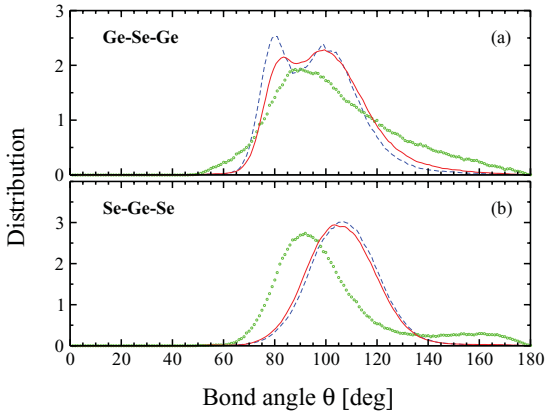

FIG. 8. (Color online) The calculated bond-angle distributions θ_{GeSeGe} and θ_{SeGeSe} for liquid Ge_2Se_3 (solid red curves), liquid $GeSe_2$ (Ref. 19) (broken blue curves) and liquid GeSe (Ref. 10) (green symbols).

(6.3%), threefold (32.6%), and fivefold (15.5%) coordinated Ge atoms.[10] The BLYP results for l-GeSe give comparable fractions of Ge-centered units at 42.7%, 6.2%, 31.5%, and 13.9%, respectively (Table IV).

E. Ring statistics

The connectivity profiles shown in Fig. 9 were evaluated by employing the Rigorous Investigation of Networks Generated using Simulation (RINGS) code[51,52] with Ge-Ge, Ge-Se, and Se-Se cutoff distances of 2.9 Å. The analysis was performed by making a King[53]-Franzblau[54] shortest path search to find rings containing a maximum of 30 atoms. Two search modes were employed using (i) each and every atom as the starting point to begin a search or (ii) only Ge atoms as the starting point to begin a search. Homopolar bonds were not excluded from the search procedure. We define $R_c(n)$ as the number of rings containing n atoms (Ge or Se) and $P_n(n)$ as the number of atoms that can be used as the origin of search for at least one ring containing n atoms. Both quantities are normalized to the total number of atoms in our model. For a given atom in an n-fold ring, $P_{min}(n)$ gives the probability that this ring is the shortest closed path having this same atom as the starting point of a search. In a similar way, $P_{max}(n)$ gives the probability that this ring is the longest closed path having this same atom as the starting point of a search.

Figure 9 shows that odd-membered rings containing between 3 and 29 atoms occur in all sizes, a result of the presence of Ge-Ge homopolar bonds, and to a lesser extent, Se-Se homopolar bonds. Two peaks are observed in $R_c(n)$ [Fig. 9(a)], the first corresponding to rings containing between four and six atoms and the second to rings containing between 14 and 22 atoms. $P_n(n)$ is helpful in capturing additional features of the network since its profile is not necessarily similar to the profile of $R_c(n)$. In particular, $P_n(n)$ shows that rings containing four to six atoms are the most significant since they constitute the shortest paths for at least a third of all atoms [see Fig. 9(b)].

$P_{max}(n)$ and $P_{min}(n)$ are useful tools in gathering information on the homogeneity of the network of rings in l-Ge_2Se_3. The low values of $P_{max}(n)$ for small ring sizes [see Fig. 9(c)]

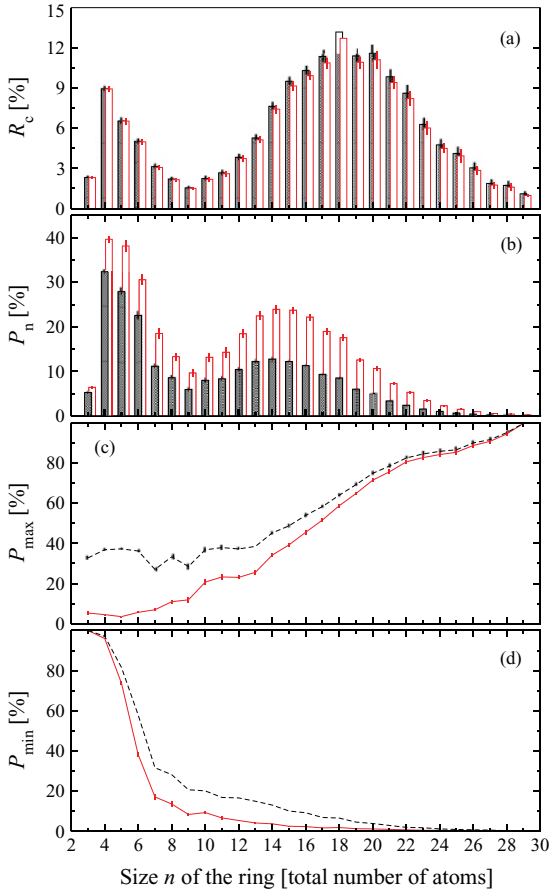

FIG. 9. (Color online) Connectivity profiles for liquid Ge_2Se_3 calculated using the RINGS method.[51,52] The profiles obtained by using both Ge and Se atoms to start a search are given in light (red) and the profiles obtained by using only Ge atoms to start a search are given in dark (black). (a) $R_c(n)$, number of rings of size n normalized to the total number of atoms in the model; (b) $P_n(n)$, number of atoms at the origin of at least one ring of size n normalized to the total number of atoms in the model; (c) $P_{max}(n)$, probability that a ring of size n is the longest closed path solution of the analysis; (d) $P_{min}(n)$, probability that a ring of size n is the shortest closed path solution of the analysis.

show that no region of the network is made from small rings alone. Conversely, the low values of $P_{min}(n)$ for large ring sizes [see Fig. 9(d)] show that no region of the network is made from large rings alone.

Using the ring statistics results, one can extract the fraction of Ge atoms not belonging to any fourfold ring, Ge(0), the fraction of Ge atoms belonging to one fourfold ring, Ge(1), and the fraction of Ge atoms belonging to two fourfold rings, Ge(2), where fourfold rings correspond to edge-sharing units.[17] In the case of l-Ge_2Se_3, the fractions of Ge(0)-, Ge(1)-, and Ge(2)-type atoms are 69%, 26%, and 5%, respectively, while in the case of l-$GeSe_2$, the fractions are 61%, 34%, and 5%, respectively.[19] The smaller fraction of edge-sharing connections in l-Ge_2Se_3 relative to l-$GeSe_2$ is consistent with the relative intensity of the two peaks in the corresponding Ge-Se-Ge bond-angle distributions, a higher first peak being observed in the bond-angle distribution for l-$GeSe_2$ [see Fig. 8(a)].

The chemical compositions of rings containing $n = n(\mathrm{Ge}) + n(\mathrm{Se})$ atoms are listed in Table V, where $n(\mathrm{Ge})$ and $n(\mathrm{Se})$ represent the number of Ge and Se atoms in a ring, respectively. For $n \leqslant 12$, the majority of even-membered rings are characterized by $n(\mathrm{Ge}) = n/2$. For larger even-membered rings, the occurrence of homopolar Ge-Ge bonds alters the chemical order such that the majority are characterized by $n(\mathrm{Ge}) = (n/2 + 1)$. For instance, when $n = 20$, 46.4% of the rings host 11 Ge atoms against 42.5% with 10 Ge atoms, and this effect is enhanced for $n > 20$. In the case of odd-membered rings, the majority are characterized by $n(\mathrm{Ge}) = (n + 1)/2$. This remains true for all ring sizes even though, with increasing size, there are increasing populations of odd-membered rings containing $n(\mathrm{Ge}) = (n + 1)/2 + 1$ and $n(\mathrm{Ge}) = (n + 1)/2 + 2$. As an example, when $n = 23$, 54.7% of rings contain $(n + 1)/2 = 12$ Ge atoms, 34.9% of rings contain $(n + 1)/2 + 1 = 13$ Ge atoms, and 2.7% of rings contain $(n + 1)/2 + 2 = 14$ Ge atoms. Overall, the chemical composition of the rings further exemplifies the role played by Ge-Ge homopolar bonds, which occur in both even- and odd-membered rings and are particularly numerous in large ring structures.

VI. INTERPLAY BETWEEN STRUCTURAL, DYNAMICAL, AND ELECTRONIC PROPERTIES

The atomic mobility is affected by the topology of a network. For instance, in the case of l-$GeSe_2$, a marked increase in chemical order is observed when adopting a polarizable ionic model in place of a first-principles model and the accompanying enhancement of the tetrahedral ordering leads to a decrease of the Ge and Se self-diffusion coefficients, D_{Ge} and D_{Se}, by one order of magnitude.[55] This tendency for departures from tetrahedral ordering to enhance the diffusion coefficients is supported by FPMD simulations of the same system using different exchange-correlation functionals.[19] It is of interest to ascertain whether these considerations apply to the case of l-Ge_2Se_3, in which tetrahedral motifs exist together with a large number of Ge-Ge homopolar bonds and Ge atoms that are not fourfold coordinated.

For this purpose, we have calculated the statistical average of the mean-square displacement of chemical species α,

$$\left\langle r_\alpha^2(t)\right\rangle = \frac{1}{N_\alpha}\left\langle \sum_{i=1}^{N_\alpha} |\mathbf{r}_{i\alpha}(t) - \mathbf{r}_{i\alpha}(0)|^2 \right\rangle, \tag{6}$$

where $\mathbf{r}_{i\alpha}(t)$ is the coordinate of the ith particle of chemical species α at time t and N_α is the total number of particles of type α. The mean-square displacements calculated for the Ge and Se atoms are shown in the inset to Fig. 10. Provided the diffusive regime is attained, the diffusion coefficient is given by

$$D_\alpha = \frac{\left\langle r_\alpha^2(t)\right\rangle}{6t} \tag{7}$$

such that a plot of $\log\langle r_\alpha^2(t)\rangle$ vs $\log t$ should show linear behavior in the long time limit with a gradient equal to unity. The values of D_{Ge} and D_{Se} that were obtained for l-Ge_2Se_3 (see Fig. 10) are summarized in Table VI where a comparison is made with the values obtained from FPMD

TABLE V. The percentage of n-membered rings containing a number n(Ge) of Ge atoms. For example, when $n = 9$, 13.5% of the rings contain four Ge atoms and 80.6% of the rings contain five Ge atoms. The number of Se atoms in an n-membered ring is given by $n(\text{Se}) = n - n(\text{Ge})$.

	Total number of atoms n in a ring																										
n(Ge)	3	4	5	6	7	8	9	10	11	12	13	14	15	16	17	18	19	20	21	22	23	24	25	26	27	28	29
1	17.9	0.1																									
2	81.9	98.3	8.5	0.4	0.1																						
3	0.1	1.6	90.6	81.5	6.6	0.9	0.2																				
4			0.9	17.9	87.8	79.5	13.5	1.5	0.4																		
5				0.2	5.5	19.5	80.6	68.6	12.9	2.1	0.4	0.1															
6						0.2	5.8	29.8	77.4	54.9	8.2	1.5	0.5	0.1													
7								0.1	9.3	41.5	74.0	40.6	7.3	1.7	0.5	0.1	0.1										
8									0.1	1.5	17.1	54.2	68.7	39.6	8.1	1.9	0.6	0.2									
9											0.2	3.5	22.5	51.4	65.1	40.7	8.4	2.0	0.7	0.2	0.1						
10												0.1	1.0	7.1	24.8	48.8	62.6	42.5	7.4	2.4	0.6	0.2					
11														0.1	1.5	8.0	26.2	46.4	63.7	39.4	6.8	2.1	0.6	0.3	0.1		
12																0.4	2.0	8.3	24.8	47.2	54.7	35.9	8.7	2.4	1.2	0.3	0.1
13																	0.1	0.5	3.2	9.9	34.9	50.5	55.0	31.3	9.4	3.8	2.3
14																			0.1	0.9	2.7	10.5	31.9	51.7	49.9	30.6	7.0
15																					0.1	0.8	3.4	13.2	35.1	51.1	45.4
16																							0.3	1.1	4.2	13.5	38.9
17																								0.1	0.1	0.8	6.2

models of l-$GeSe_2$ (Ref. 19) and l-GeSe.[10] In l-Ge_2Se_3, the Ge atoms are more mobile than the Se atoms, both species being more mobile than in l-$GeSe_2$ but less mobile than in l-GeSe. Comparison with the structures of l-$GeSe_2$ (Ref. 19), l-Ge_2Se_3 (see Table IV), and l-GeSe (Ref. 10) shows that the increase of the diffusion coefficients in l-Ge_xSe_{1-x} with x increasing from 0.33 to 0.5 is consistent with the destabilization of a network based on Ge-Se_4 tetrahedral motifs caused by an increasing fraction of Ge-Ge homopolar bonds and by the appearance of non-negligible proportions of threefold and fivefold Ge-centered units.

In recent work, we compared the performances of two DFT models for l-$GeSe_2$ that differed in the exchange-correlation part of the DFT functional.[19,36] A clear correlation was found between increased tetrahedral ordering and the appearance of a deeper pseudogap around the Fermi level in the electronic density of states. The question arises as to the existence of such a correlation when the tetrahedral order is modified by a change in concentration within the family of Ge_xSe_{1-x} liquids. We address this issue in Fig. 11 by comparing the calculated electronic density of states (EDOS) for l-Ge_2Se_3 and l-$GeSe_2$. In the present case, 50 independent configurations were extracted from the whole equilibrium trajectory and were used to make the statistical average. It appears that the bonding in l-Ge_2Se_3 features an enhanced metallic character, as exemplified by a less pronounced pseudogap around the Fermi level. This behavior is consistent with the development in l-Ge_xSe_{1-x} of a fully metallic character for liquid Ge.[56,57] From the methodological point of view, the existence of a vanishing pseudogap calls for an accurate control of the stability of the first-principles Car-Parrinello trajectories, known to be highly sensitive to any band-closing tendency. Careful use and tuning of the parameters associated with the electronic part of the Nosé-Hoover thermostats ensured that the total Hamiltonian of the system was well conserved, with fluctuations having an amplitude smaller than 0.001% at thermal equilibrium.[38–40]

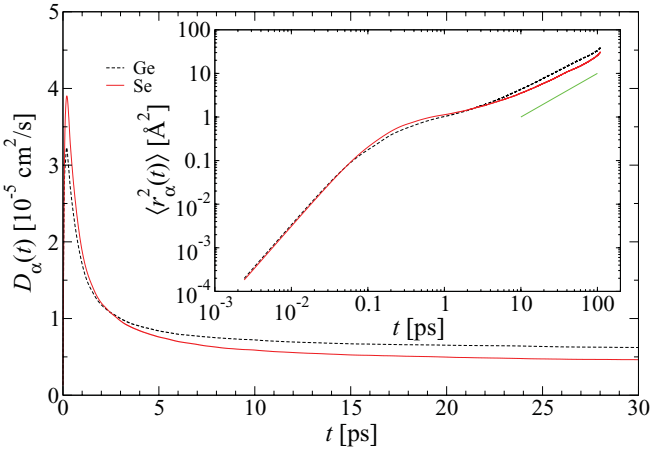

FIG. 10. (Color online) The diffusion coefficients of Ge atoms (broken black curve) and Se atoms (solid red curve) in liquid Ge_2Se_3 at $T = 1000$ K as calculated from the mean-square displacement of a given chemical species at time t [see Eq. (7)]. The inset shows the time dependence of the mean-square displacements of the Ge atoms (broken black curve) and the Se atoms (solid red curve), and the straight green line indicates the slope corresponding to the diffusive regime.

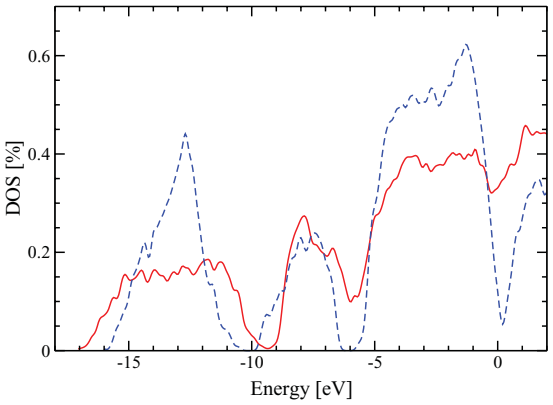

FIG. 11. (Color online) The electronic density of states extracted from the Kohn-Sham eigenvalues. The result for liquid Ge_2Se_3 (solid red curve) is compared with that obtained for liquid $GeSe_2$ (broken blue curve) (Ref. 19). A Gaussian broadening of 0.1 eV has been employed.

VII. CONCLUSION

Liquids belonging to the Ge_xSe_{1-x} family display a variety of structural features, including the presence of chains of Se atoms (or n-mers) in l-Se,[58–60] the connection by Ge-centered tetrahedra of Se atoms arranged in n-mers for l-$GeSe_4$,[7] the creation of a defected tetrahedral network for l-$GeSe_2$,[2,12,19] the coexistence of a variety of Ge and Se centered structural motifs in l-GeSe,[9,10] and the establishment of metallic bonding in liquid Ge.[56,57] In the present work we have focused on liquid Ge_2Se_3, a system which is representative of the range of concentrations between l-$GeSe_2$ and l-GeSe and which lies at the edge of the glass-forming region in the Ge_xSe_{1-x} system.[31]

Our first-principles model of l-Ge_2Se_3 was validated by comparison with the available neutron diffraction results in both real and reciprocal space. The FSDP in the measured total structure factor at $\simeq 1$ $Å^{-1}$ was then identified with intermediate range order associated with the Ge-Ge correlations. The main Ge-centered structural units, which link to form this IRO, were found to be Ge-Se_4 and Ge-$GeSe_3$ tetrahedra, while the majority of Se atoms were found to be twofold coordinated in Se-Ge_2 configurations. The model also contains a large number of miscoordinated units involving Ge and Se atoms that are not fourfold and twofold coordinated, respectively, where Ge-Se_3 and Se-Ge_3 units are typical examples. The bond-angle

TABLE VI. The diffusion coefficients of the Ge and Se atoms in the liquids $GeSe_2$, Ge_2Se_3, and GeSe as obtained from FPMD models.

	D_α ($\times 10^{-5}$ cm^2/s)	
	Ge	Se
l-$GeSe_2$ (Ref. 19)	0.2 ± 0.2	0.2 ± 0.2
l-Ge_2Se_3 (present work)	0.62 ± 0.2	0.46 ± 0.2
l-GeSe (Ref. 10)	2.8 ± 0.3	2.0 ± 0.3

distributions and the ring statistics show the occurrence of both edge-sharing and corner-sharing Ge-centered units, the former being less numerous than in l-$GeSe_2$. The impact of Ge-Ge homopolar bonds is clearly visible in the ring statistics which show that these connections occur in both even- and odd-membered rings and are particularly numerous in large ring structures.

The neutron diffraction and first-principles molecular dynamics results for liquid Ge_xSe_{1-x} both show substantial changes in the structure on changing the composition from Ge_2Se_3 to GeSe. Both systems lie on the Ge-rich side of the composition range and therefore contain structural motifs other than tetrahedral Ge-Se_4 units. However, there are marked differences in a number of properties such as the coordination numbers and the low k behavior of the Faber-Ziman Ge-Ge and Bhatia-Thornton NN and NC partial structure factors, where an FSDP appears in the case of l-Ge_2Se_3. In the case of l-Ge_2Se_3, the results show that the network is made predominantly from an arrangement of Ge-centered tetrahedral units in which the 8-N rule is largely obeyed, i.e., most Ge atoms are fourfold coordinated and most Se atoms are twofold coordinated. By contrast, in the case of l-GeSe, the results do not show any predominant tetrahedral motif and the 8-N rule is not obeyed. Thus the relative fractions of the different structural units most likely provide the key quantity for appreciating the differences between these two liquids. Fourfold tetrahedral arrangements of Ge atoms are favored in the case of Ge_2Se_3, while there is a much wider distribution of structural units in the case of GeSe.

Finally, the increase of the diffusion coefficients in l-Ge_xSe_{1-x} with x increasing from 0.33 to 0.5 is consistent with the destabilization of a network based on Ge-Se_4 tetrahedral motifs caused by an increasing fraction of Ge-Ge homopolar bonds and by the appearance of non-negligible proportions of threefold and fivefold Ge-centered units. A further fingerprint of incomplete tetrahedral order is provided by the behavior of the electronic density of states, which exhibits more metallic-like characteristics in the vicinity of the Fermi level when compared to l-$GeSe_2$. The preparation of a model for glassy Ge_2Se_3, to be compared with the available experimental results, is currently in progress.

ACKNOWLEDGMENTS

This work was granted access by GENCI (Grand Equipement National de Calcul Intensif) under allocation 2011095071 to the HPC resources of CCRT/CINES/IDRIS.

[1] I. T. Penfold and P. S. Salmon, J. Phys.: Condens. Matter **2**, SA233 (1990).
[2] I. T. Penfold and P. S. Salmon, Phys. Rev. Lett. **67**, 97 (1991).
[3] P. S. Salmon and J. Liu, J. Phys.: Condens. Matter **6**, 1449 (1994).
[4] K. Maruyama, M. Misawa, M. Inui, S. Takeda, Y. Kawakita, and S. Tamaki, J. Non-Cryst. Solids **205–207**, 106 (1996).
[5] M. Cobb, D. A. Drabold, and R. L. Cappelletti, Phys. Rev. B **54**, 12162 (1996).
[6] C. Massobrio, A. Pasquarello, and R. Car, Phys. Rev. Lett. **80**, 2342 (1998).
[7] M. J. Haye, C. Massobrio, A. Pasquarello, A. De Vita, S. W. de Leeuw, and R. Car, Phys. Rev. B **58**, R14661 (1998).
[8] I. Petri, P. S. Salmon, and H. E. Fischer, J. Non-Cryst. Solids **250–252**, 405 (1999).
[9] I. Petri, P. S. Salmon, and H. E. Fischer, J. Phys.: Condens. Matter **11**, 7051 (1999).
[10] F. H. M. van Roon, C. Massobrio, E. de Wolff, and S. W. de Leeuw, J. Chem. Phys. **113**, 5425 (2000).
[11] C. Massobrio, A. Pasquarello, and R. Car, Phys. Rev. B **64**, 144205 (2001).
[12] P. S. Salmon and I. Petri, J. Phys.: Condens. Matter **15**, S1509 (2003).
[13] D. N. Tafen and D. A. Drabold, Phys. Rev. B **71**, 054206 (2005).
[14] E. Bychkov, C. J. Benmore, and D. L. Price, Phys. Rev. B **72**, 172107 (2005).
[15] P. S. Salmon, J. Non-Cryst. Solids **353**, 2959 (2007).
[16] F. Inam, M. T. Shatnawi, D. Tafen, S. J. L. Billinge, P. Chen, and D. A. Drabold, J. Phys.: Condens. Matter **19**, 455206 (2007).
[17] C. Massobrio and A. Pasquarello, Phys. Rev. B **77**, 144207 (2008).
[18] M. T. M. Shatnawi, C. L. Farrow, P. Chen, P. Boolchand, A. Sartbaeva, M. F. Thorpe, and S. J. L. Billinge, Phys. Rev. B **77**, 094134 (2008).
[19] M. Micoulaut, R. Vuilleumier, and C. Massobrio, Phys. Rev. B **79**, 214205 (2009).
[20] C. Massobrio, M. Celino, P. S. Salmon, R. A. Martin, M. Micoulaut, and A. Pasquarello, Phys. Rev. B **79**, 174201 (2009).
[21] G. Chen, F. Inam, and D. A. Drabold, Appl. Phys. Lett. **97**, 131901 (2010).
[22] X. Feng, W. J. Bresser, and P. Boolchand, Phys. Rev. Lett. **78**, 4422 (1997).
[23] P. S. Salmon, Proc. R. Soc. London, Ser. A **445**, 351 (1994).
[24] C. Massobrio, A. Pasquarello, and R. Car, J. Am. Chem. Soc. **121**, 2943 (1999).
[25] C. Massobrio, F. H. M. van Roon, A. Pasquarello, and S. W. De Leeuw, J. Phys.: Condens. Matter **12**, L697 (2000).
[26] C. Massobrio and A. Pasquarello, J. Chem. Phys. **114**, 7976 (2001).
[27] C. Massobrio and A. Pasquarello, Phys. Rev. B **68**, 020201 (2003).
[28] C. Massobrio, M. Celino, and A. Pasquarello, Phys. Rev. B **70**, 174202 (2004).
[29] C. Massobrio and A. Pasquarello, Phys. Rev. B **75**, 014206 (2007).
[30] L. Giacomazzi, C. Massobrio, and A. Pasquarello, Phys. Rev. B **75**, 174207 (2007).
[31] R. Azoulay, H. Thibierge, and A. Brenac, J. Non-Cryst. Solids **18**, 33 (1975).
[32] R. Car and M. Parrinello, Phys. Rev. Lett. **55**, 2471 (1985).
[33] A. D. Becke, Phys. Rev. A **38**, 3098 (1988).
[34] C. Lee, W. Yang, and R. G. Parr, Phys. Rev. B **37**, 785 (1988).
[35] C. Massobrio, M. Micoulaut, and P. S. Salmon, Solid State Sci. **12**, 199 (2010).
[36] M. Micoulaut and C. Massobrio, J. Optoelectron. Adv. Mater. **11**, 1907 (2009).
[37] N. Troullier and J. L. Martins, Phys. Rev. B **43**, 1993 (1991).
[38] S. Nosé, Mol. Phys. **52**, 255 (1984).

[39]W. G. Hoover, Phys. Rev. A **31**, 1695 (1985).
[40]P. E. Blöchl and M. Parrinello, Phys. Rev. B **45**, 9413 (1992).
[41]A. B. Bhatia and D. E. Thornton, Phys. Rev. B **2**, 3004 (1970).
[42]H. E. Fischer, A. C. Barnes, and P. S. Salmon, Rep. Prog. Phys. **69**, 233 (2006), describe the relationship between the three sets of partial structure factors commonly used (Faber-Ziman, Ashcroft-Langreth, and Bhatia-Thornton).
[43]P. S. Salmon, Proc. R. Soc. London, Ser. A **437**, 591 (1992).
[44]J. Ruska and H. Thurn, J. Non-Cryst. Solids **22**, 277 (1976).
[45]T. Okada, T. Satoh, M. Matsumura, and S. Ohno, J. Phys. Soc. Jpn. **65**, 230 (1996).
[46]S. Le Roux and C. Massobrio (unpublished).
[47]C. N. J. Wagner and H. Ruppersberg, At. Energy Rev. **1**, 101 (1981).
[48]P. Chieux and H. Ruppersberg, J. Phys. Coll. **41**, C8 (1980), discuss the case when $S_{NC}(k) = 0$ which corresponds to $g_{NC}(r) = 0$. Then $c_{Ge}g_{GeGe}(r) + c_{Se}g_{GeSe}(r) = c_{Se}g_{SeSe}(r) + c_{Ge}g_{SeGe}(r)$ for all r values and $\bar{n}_{Ge} = \bar{n}_{Se}$ such that the generalized Warren-Cowley short-range chemical order parameter reduces to the more usual expression $\alpha'_w = 1 - \bar{n}_{GeSe}/c_{Se}\bar{n} = (4\pi n_0/\bar{n})\int_{r_1}^{r_2} dr\, g_{CC}(r)r^2$, where r_1 and r_2 denote the minima on either side of the first peak in $g_{CC}(r)$. Since $g_{CC}(r) = c_{Ge}c_{Se}\,[g_{GeGe}(r) + g_{SeSe}(r) - 2g_{GeSe}(r)]$, a preference for heteropolar bonds corresponds to $\alpha'_w < 0$, whereas a preference for homopolar bonds corresponds to $\alpha'_w > 0$.
[49]G. S. Cargill III and F. Spaepen, J. Non-Cryst. Solids **43**, 91 (1981).
[50]M. Maret, P. Chieux, P. Hicter, M. Atzmon, and W. L. Johnson, J. Phys. F **17**, 315 (1987).
[51]S. Le Roux and P. Jund, Comput. Mater. Sci. **49**, 70 (2010).
[52]S. Le Roux and P. Jund, Comput. Mater. Sci. **50**, 1217 (2011).
[53]S. V. King, Nature (London) **213**, 1112 (1967).
[54]D. S. Franzblau, Phys. Rev. B **44**, 4925 (1991).
[55]M. Wilson, B. K. Sharma, and C. Massobrio, J. Chem. Phys. **128**, 244505 (2008).
[56]P. S. Salmon, J. Phys. F **18**, 2345 (1988).
[57]S. Munejiri, T. Masaki, T. Itami, F. Shimojo, and K. Hoshino, Phys. Rev. B **77**, 014206 (2008).
[58]R. Bellissent and G. Tourand, J. Non-Cryst. Solids **35–36**, 1221 (1980).
[59]D. Hohl and R. O. Jones, Phys. Rev. B **43**, 3856 (1991).
[60]G. Kresse, F. Kirchhoff, and M. J. Gillan, Phys. Rev. B **59**, 3501 (1999).